Full Paper | http://dx.doi.org/10.17807/orbital.v13i3.1567

Supporting information for

Photocatalytic Activity and Antibacterial Effect of Ag_3PO_4 Powders Against Methicillin-resistant *Staphylococcus aureus*

Gleice Botelho* [a], Camila Cristina de Foggi [b], Carlos Eduardo Vergani [b], Wyllamanney Silva Pereira [c], Ricardo kaminishi dos Santos Júnior [a], Elson Longo [c]

[a.] Department of Environmental Chemistry, Federal University of Tocantins, 77402-970, Gurupi, TO, Brazil.
[b.] São Paulo State University (UNESP) - Department of Dental Materials and Prosthodontics, P.O. Box 355, 14801-903, Araraquara, SP, Brazil
[c.] INCTMN-UFSCar, Federal University of São Carlos, P.O. Box 676, 13565-905, São Carlos, SP, Brazil.

Supplementary Information

The Rietveld Method

Ag_3PO_4 powder was analyzed according to the Rietveld method [1], using the general structure analysis (GSAS) software with the EXPGUI graphical interface [2]. The input data for the theoretical model was that in ICSD 14000 [3]. In this analysis, the refined parameters were the scale factor, background, shift lattice constants, profile half-width parameters (u, v, and w), isotropic thermal parameters, lattice parameters, strain anisotropy factor, preferential orientation, and atomic functional positions. The background fitted was performed using the Chebyschev polynomial of the first kind. The peak profile function was modeled using a convolution of the Thompson−Cox−Hastings pseudo-Voigt (TCH-pV) [4] with the asymmetry function described by Finger [5].

Figure S1 shows the experimentally observed and theoretically calculated XRD patterns of Ag_3PO_4. The difference between the two XRD patterns (the residual pattern) shows a good fit, noted by the small variation in the intensity scale, as illustrated by the Obs–Calc line. The inset of Figure S1 shows a schematic representation of a cubic Ag_3PO_4 unit cell. This representation was modeled using the Diamond crystal and molecular structure visualization software using the lattice parameters and atomic positions obtained from the Rietveld refinement (Table S1). In this cubic structure, P and Ag cations are coordinated to four O atoms, which form and $[AgO_4]$ clusters with tetrahedral configurations [6].

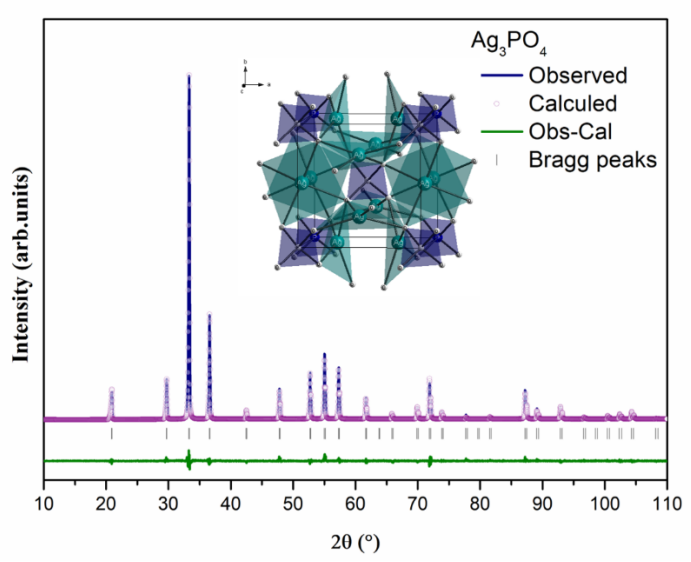

Figure S1. Rietveld refinements of the Ag_3PO_4 powder.

The statistical parameters (R_{wp}, R_p, R_{Bragg}, and χ^2) illustrated in Table S1 indicate a good quality of the structural refinements. The positions of the Ag and P atoms in the Ag_3PO_4 powder were fixed; however, the positions of the O atoms presented some variations, because the O atoms in this structure did not occupy fixed positions. The lattice parameters and unit cell volumes values were in agreement with the values reported in the literature and ICSD 14000, and as expected the Ag_3PO_4 sample was crystalized in a body-centered cubic structure with $P\bar{4}3n$ space group and two molecular formula units per unit cell (Z = 2) [3,6].

Table S1. Rietveld refinement results for the Ag_3PO_4 powder.

Atom	Wyckoff	X	Y	Z
Ag	6d	0.25	0	0.50
P	2a	0	0	0
O	8e	0.147557	0.147557	0.147557

$a = 6.014(7)$Å; $V = 217.591(4)$Å^3; $R_{wp} = 14.38\%$; $R_p = 9.30\%$; $R_{Bragg} = 4.98\%$;

$\chi^2 = 1.2165$.

Table S2 shows the bond angles and lengths associated with isolated $[AgO_4]$ and clusters, as well as combinations. The $[AgO_4]$ clusters are highly distorted in the lattice as indicated by the existence of two O–Ag–O bond angles (α and β). In Ag_3PO_4, the distorted tetrahedral $[AgO_4]$ clusters are caused by the inductive effect of the highly electronegative PO_4^{3-} group. This inductive effect is described as the action of one group electrostatically affecting the electron distribution in another group, in our case the cluster against the $[AgO_4]$ clusters [6,7].

Table S2. Bond angles and lengths for the [AgO_4] and [AgO_4] clusters.

Sample	Bond lengths (Å)		Bond Angles (°)				
	Ag-O	P-O	O-Ag-O		O-P-O	Ag-O-Ag	P-O-Ag
			α	*B*	*Δ*	*ε*	*γ*
Ag_3PO_4	2.37	1.53	93.84	149.99	109.47	101.44	116.64
Ag_3PO_4 – CIF 14000	2.37	1.55	93.78	150.23	109.47	101.71	116.41

Average particle size distribution

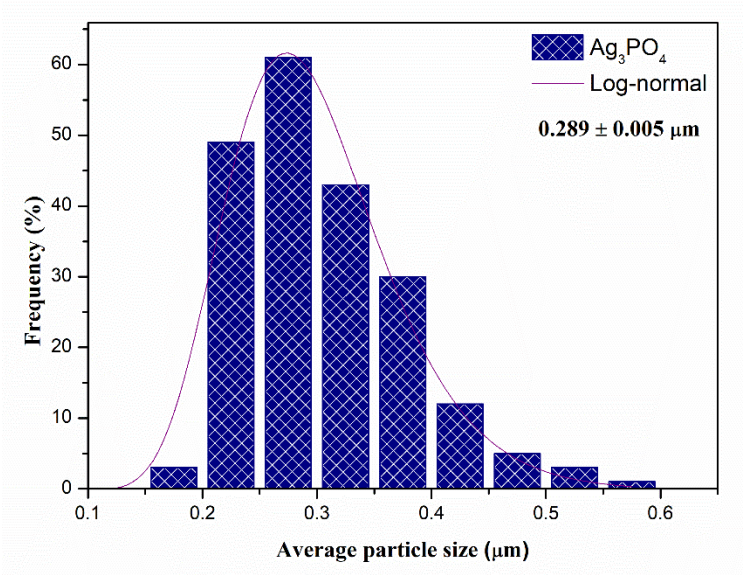

Figure S2. Average particle size distribution for the Ag_3PO_4 powder.

UV–Vis Absorption Spectroscopy Analysis

The optical band gap energy of Ag_3PO_4 was experimentally estimated utilizing the Wood and Tauc method [9], using the following equation:

$$\alpha h\nu = A(h\nu - E_{gap})^n \quad \text{.....(S1)}$$

where h is Plank's constant, ν is the frequency of vibration, α is the absorption coefficient, E_{gap} is the band gap energy, and A a proportional constant. The value of the exponent n denotes the nature of the electronic transitions. The existing literature explained that Ag_3PO_4 presents an optical absorption due to the indirectly allowed electronic transitions (n=2) [6,10].

The diffuse reflectance measurement can be converted using the Kubelka–Munk (K–M) function [11], represented by $F(R_\infty)$:

$$F(R_\infty) = \frac{(1-R_\infty)^2}{2R_\infty} = \frac{K}{S} \quad \text{.....(S2)}$$

where k is the molar absorption coefficient, S is the scattering coefficient, and $R_\infty = \frac{R_{sample}}{R_{MgO}}$, is the reflectance when the sample is infinitely thick. In our study, we adopted magnesium oxide (MgO) as the standard sample for reflectance measurements. Thus, the vertical axis was converted to $F(R\infty)$, which is proportional to the absorption coefficient. Subsequently, substituting α in the Tauc equation for $F(R\infty)$, we obtained the modified K–M equation:

$$(F(R_\infty)\mathrm{h}\nu)^{1/2} = \mathrm{A}(\mathrm{h}\nu - \mathrm{E_{gap}}) \quad \text{.....(S3)}$$

Therefore, when plotting $(F(R_\infty)\mathrm{h}\nu)^{1/2}$ against $h\nu$ (Figure S3), E_{gap} corresponds to the $h\nu$ value at the intersection of the line tangent to the graph with the horizontal axis.

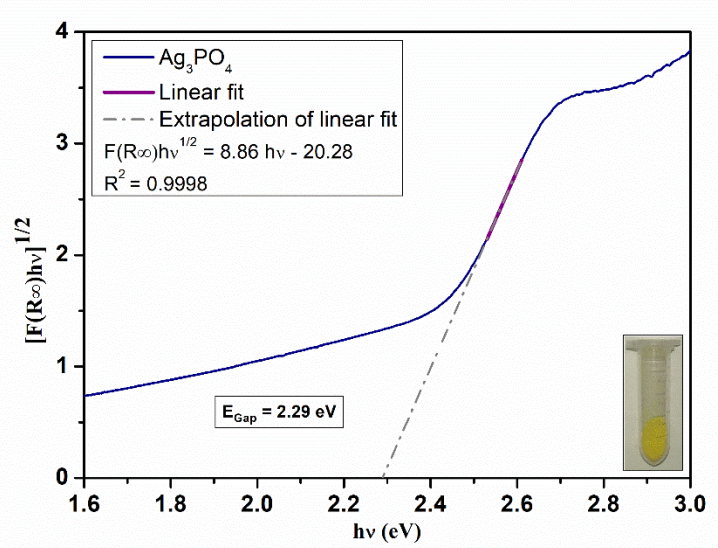

Figure S3. UV–Vis DRS spectrum of the Ag_3PO_4 powder. The inset shows a digital image of the yellow Ag_3PO_4 powder.

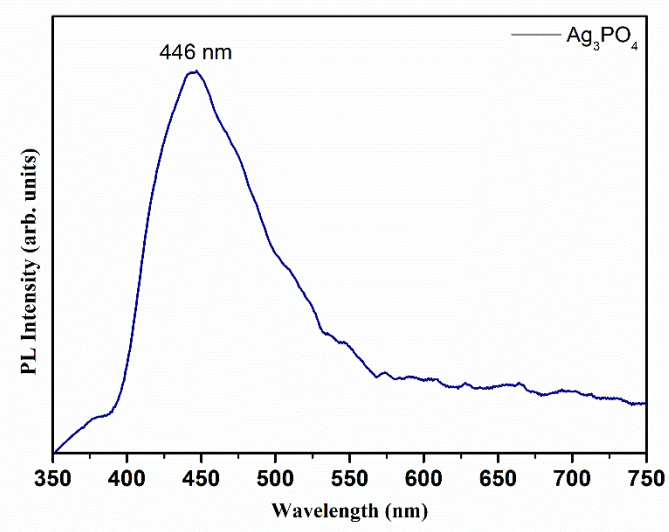

Figure S4. PL spectrum of the Ag_3PO_4 powder.

References

[1] Rietveld H. *J. Appl. Crystallogr*. **1969**, 2 (2), 65. https://doi.org/10.1107/S0021889869006558

[2] Toby B. H. *J. Appl. Crystallogr*. **2001**, 34 (2), 210. https://doi.org/10.1107/S0021889801002242

[3] Masse R.; Tordjman I.; Durif A. *Z. Kristallogr*. **1976**, 144 (1-2), 76. https://doi.org/10.1524/zkri.1976.144.1-6.76

[4] Thompson P.; Cox D.; Hastings J. *J. Appl. Crystallogr*. **1987**, 20 (2), 79. https://doi.org/10.1107/S0021889887087090

[5] Finger L.; Cox D.; Jephcoat A. *J. Appl. Crystallogr.* **1994**, 27 (6), 892. https://doi.org/10.1107/S0021889894004218

[6] Ma X.; Lu B.; Li D.; Shi R.; Pan C.; Zhu Y. *J. Phys. Chem. C.* **2011**, 115 (11), 4680. https://doi.org/10.1021/jp111167u

[7] Zaghib K.; Julien C. *J. Power Sources*. **2005**, 142 (1-2), 279. https://doi.org/10.1016/j.jpowsour.2004.09.042

[8] Ayed B. *CR Chimie*. **2012**, 15 (7), 603. https://doi.org/10.1016/j.crci.2012.05.007

[9] Wood D.; Tauc J. *Phys. Rev. B* **1972,** 5 (8), 3144. https://doi.org/10.1103/PhysRevB.5.3144

[10] Botelho G.; Sczancoski J. C.; Andres J.; Gracia L.; Longo E. *J. Phys. Chem. C.* **2015**, 119 (11), 6293. https://doi.org/10.1021/jp512111v

[11] Tolvaj L.; Mitsui K.; Varga D. *Wood Sci. Technol.* **2011**, 45 (1), 135. https://doi.org/10.1007/s00226-010-0314-x